Dynamics of Water Intercalated in Graphite Oxide

Silvina Cerveny,*,† Fabienne Barroso-Bujans,† Ángel Alegría,†,‡ and Juan Colmenero†,§

Centro de Fisica de Materiales (CSIC, UPV/EHU)-Materials Physics Center, Paseo Manuel de Lardizabal 4, 20018, San Sebastián, Spain, Departamento de Física de Materiales, UPV/EHU, Facultad de Química, Apartado 1072, 20018, San Sebastián, Spain, and Donostia International Physics Center, San Sebastián, Spain

Received: August 18, 2009; Revised Manuscript Received: December 24, 2009

Intercalated water in graphite oxide (GO) was investigated by using different techniques: broadband dielectric spectroscopy (BDS) ($10^{-2}-10^{9}$ Hz; 140−300 K), differential scanning calorimetry, X-ray diffraction, and attenuated total reflection geometry in Fourier transform infrared spectroscopy (ATR-FTIR). We have studied the water concentration (c_w) region from 0 wt % (anhydrous GO) up to 25 wt % since in this range the water crystallization is avoidable. The interlayer distance during hydration increases from 5.67 to 8 Å which corresponds to the uptake of a water monolayer in the interlayer space of GO. A clear relaxation due to water molecule reorientation is seen by BDS. The rotational water dynamics is dependent on the hydration level. At high water concentration (c_w > 15 wt %), water−water interactions seem to dominate the dielectric response. This result is also compatible with those from FTIR and X-ray measurements. In this water concentration region, a slight dynamical crossover in the temperature dependence of the relaxation times is observed. We show that the crossover temperature on this system (T_{cross}) depends on the confinement size.

1. Introduction

The study of atoms, molecules, and macromolecules geometrically confined on a nanometric scale has shown a growing interest from the seminal works in the seventies[1–4] until the recent works in refs 5–8. Different reasons arise for studying the behavior of confined materials. On one hand, confined systems are potential applications of new materials, which mimic the function of natural systems, which have significant relevance in several fields from energy systems to biological sensors. On the other hand, confinement induces unusual structural and dynamic properties which can be used to explore many attractive and sometimes unexpected physical problems.

Water is an ideal candidate to be studied on a nanoscale since several important phenomena, for instance, in cell membranes, take place in a nanoscopic water environment. Additionally, water restricted on nanometer length scales is also found in many nonbiological situations like industrial and geophysical applications. Consequently, in recent times a lot of works on confined water have appeared in the literature (see refs 7 and 9–13 and references therein). However, despite intensive study, there still remain a number of open questions. For instance, the dynamics of supercooled water is a matter of debate. Whereas at room temperatures the behavior of bulk water is fragile, at low temperature confined water seems to be strong in the Angell classification[14] of supercooled liquids. To link these two different behaviors, the so-called "fragile-to-strong" (FTS) transition was proposed to occur between 235 and 150 K.[15] Unfortunately, bulk water crystallizes at temperatures lower than 235 K due to homogeneous nucleation, and therefore, experiments of water on confined geometries became relevant to study the supercooled water dynamics at low temperatures. Thus, water has been constrained in several systems such as pore glasses,[12] regular porous silicates (MCM-41 and SBA-15),[16,17] mineral clays,[11] cements,[18] or carbon nanotubes[19] in an effort to avoid the crystallization and thus to analyze its behavior at low temperatures. Later in this work we will summarize both results and interpretations concerning water dynamics at supercooled temperatures in confined geometries.

One of the still unexplored systems to investigate confined water by broadband dielectric spectroscopy is graphite oxide (GO). GO is a layered material derived from the strong oxidation of graphite. The structural properties of GO have been investigated since 1859, when it was first produced,[20] mainly by using nuclear magnetic resonance (NMR) as well as theoretical predictions and simulations.[21–24] However, its structure still remains controversial in the literature.[23,25–28] Essentially, GO consists of graphene sheets, and depending on the oxidation method, it could contain a variable fraction of epoxide and hydroxyl groups in addition to carbonyl and carboxyl groups localized at the edges.[28] Besides, during oxidation an expansion of the interlayer distance between graphene sheets is produced. Whereas in graphite the interlayer distance is about 3.5 Å in unfilled GO, this distance grows approximately up to 6 Å.[29]

Due to the hydrophilic nature of GO, it is possible to intercalate polar organic molecules as well as polymers between the layers. In this type of compound the chemical structure of GO remains almost intact, and the guest molecules or atoms are located in between. These intercalated layered materials have attracted the interest of the scientific community due to its potential applications in the fields of batteries, biosensor technology, electromagnetic shielding, and other applications. For instance, polymers such as poly(ethylene oxide),[29] poly(vinyl alcohol),[30] poly(vinyl acetate),[31] poly(vinylpyrrolidone), methyl cellulose, poly(oxymethylene-(oxyethylene)) or poly(oligo(ethylene glycol oxalate))[32] have been intercalated into graphite oxide as well as organic ammonium ions[33] and alcohols.[29] However, as graphite oxide is extremely hydrophilic, water

* Corresponding author. E-mail: scerveny@ehu.es.
† Centro de Fisica de Materiales (CSIC, UPV/EHU)-Materials Physics Center.
‡ Departamento de Física de Materiales, UPV/EHU.
§ Donostia International Physics Center.

10.1021/jp907979v
Published on Web 01/27/2010

molecules are always trapped in the interlayer spacing of GO. For this reason, it is very interesting to study both the structure and dynamics of this intercalated water. In two previous papers,[34,35] the water dynamics in GO was studied by using a neutron scattering time-of-flight spectrometer, between 240 and 320 K and in the range from 10 to 100% of relative humidity (which correspond to interlayer distances from 7 to 11 Å). By contrast, here we have mainly analyzed the low-temperature region from 130 to 250 K by using dielectric spectroscopy.

In this work, we have investigated both the structure and the dynamics of water molecules intercalated in the interlayer of GO below the water crystallization threshold. Characterization of structural properties in dry and hydrated GO was done by X-ray diffraction. To study the water dynamics we have used broadband dielectric spectroscopy due to the high dipolar moment of water molecules. We show that water−water interactions seem to dominate the dielectric response at high hydration level as also observed by ATR-FTIR measurements. Finally, the temperature dependence of the relaxation times will be discussed and compared with that obtained for other confinement systems previously published.

2. Experimental Section

2.1. Materials. ***2.1.1. Preparation of Graphite Oxide.*** Graphite oxide was produced using natural graphite powder (universal grade, 200-mesh, 99.9995%) according to the Brodie method.[20] A reaction flask with 200 mL of fuming nitric acid was cooled to 0 °C in a cryostat bath for 20 min, and then the graphite powder (10 g) was thoroughly dispersed to avoid agglomeration. Subsequently, potassium chlorate (80 g) was slowly added over 1 h, to avoid sudden increases in temperature, and the reaction mixture was stirred for 21 h at 0 °C. Once the reaction was finished, the mixture was diluted in distilled water and filtered until the supernatant had a nitrate content lower than 1 mg/L (AQUANAL-plus nitrate (NO3) 1−50 mg/L). The GO slurry was dried at 110 °C for 72 h. After that, GO was sieved to obtain a fine powder with particles size of less than 45 μm, dried again at 110 °C for 72 h, and stored in a vacuum at room temperature until use. It is important to note that conventional TGA results in this GO show a decomposition temperature close to 230 °C[36] without any signature of degradation below 180 °C. To further analyze the thermal decomposition of our GO we also measured TGA curves at 110 °C during 6 days. As reported in the Supporting Information, the GO synthesized here loses only 1.6% mass (most likely water loss) during this treatment.

2.1.2. Preparation of Water-Intercalated GO. Hydrated GO samples with water content of 5, 10, 15, 20, 25, and 30 wt % were prepared by hydration−dehydration procedures. First, GO was hydrated in a 100% humid chamber at 35 °C for a week, reaching at maximum a 32 wt % hydration level. Subsequently, the samples were dehydrated by evaporation directly on the dielectric electrodes and immediately introduced in the dielectric spectrometer. The water content was determined by weight and confirmed by thermogravimetric analysis. A portion of the hydrated samples was immediately crimp-sealed into the DSC pans for analysis.

2.2. Experimental Techniques. Both dry and hydrated GO were characterized by powder X-ray diffraction (Philips X'Pert Pro), using Cu Kα radiation (λ = 1.54056 Å), with a back monochromator. The radiation source was operated at a generator voltage of 40 kV and a current of 40 μA. The scans were carried out with 0.026 steps, over the range from 2° to 45° (2θ) at 20 °C.

A broadband dielectric spectrometer, Novocontrol Alpha analyzer, was used to measure the complex dielectric function, $\varepsilon^*(\omega) = \varepsilon'(\omega) - i\varepsilon''(\omega)$, $\omega = 2\pi f$, in the frequency (f) range from $f = 10^{-2}$ Hz to $f = 10^6$ Hz. The samples were placed between parallel gold-plated electrodes with a diameter of 30 mm and were typically 0.4 mm thick. After fast cooling (rate >20 K/min), isothermal frequency scans recording $\varepsilon^*(\omega)$ were performed every 5° over the temperature range 130−260 K. The sample temperature was controlled with stability better than ±0.1 K. Additionally, all the samples were also measured in a higher-frequency range (10^6−10^9 Hz) by using an Agilent RF impedance analyzer 4192B. In this case, parallel gold-plated electrodes with a diameter of 10 mm were used. In addition, only for the sample with the highest water content, room-temperature dielectric measurements in the frequency range of 50 MHz−5 GHz were done by using an integrated system of an HP8361A vector network analyzer (VNA) and dielectric probe kit HP85070E with an open-ended coaxial (OEC) probe.

For differential scanning calorimeter (DSC) measurements, a Q2000 TA Instrument was used in both standard and temperature-modulated modes (TMDSC). Standard DSC measurements were performed using cooling and heating rates of 20 K/min. TMDSC experiments were carried out on heating with a temperature amplitude $T_a = 0.8$ K, a modulation period of $t_p = 60$ s, and 2 K/min of underlying heating rate. In both cases, hermetic aluminum pans were used for all the materials; the sample weights were about 7 mg; and the helium flow rate used was 25 mL/min.

The thermal stability of dry and hydrated graphite oxide was characterized by thermogravimetric analysis (TGA-Q500, TA Instruments). All measurements were conducted under high purity nitrogen flow over a temperature range of 30−350 °C with a slow ramp rate of 1 K/min to prevent sample loss due to GO exfoliation.

Fourier transform infrared spectroscopy (FTIR) was carried out by means of a JASCO 6500 spectrometer using the attenuated total reflectance method (ATR) at room temperature in the range of 4500−1000 cm^{-1}. Each spectrum was collected with a resolution of 4 cm^{-1} and an average of 150 repetitive scans. Different portions of each sample were analyzed. The spectra were baseline corrected by using the Software Spectra Analysis from Jasco, and no smoothing of the data was done.

3. Results

3.1. Structural Characterization of Dry GO. First we analyzed the chemical structure of dry GO. Elemental analysis of our GO showed an atomic composition of $C_8H_{1.38}O_{2.6}$.

Figure 1a shows the X-ray diffraction pattern of dried GO as a function of the scattering vector (Q). Three typical features are observed: one very intense and sharp peak at about Q = 1.1 $Å^{-1}$ ($2\theta = 15°$), a very broad contribution at $Q = 2.22$ $Å^{-1}$ ($2\theta = 31°$), and finally a small contribution at about $Q = 2.93$ $Å^{-1}$ ($2\theta = 43°$). The characteristic interlayer spacing was calculated as $d = 2\pi/Q_{max}$. Taking into account the most intense diffraction peak, a typical spacing of 5.67 Å was obtained for the dry sample. This interlayer distance is mainly attributed to the lamellar structure of GO, and its value is similar to that published by other authors.[34,35] The other two peaks, corresponding to a spacing of 2.85 and 2.13 Å, were also reported in the literature.[37]

The type of functional groups in dry GO has been characterized by using ^{13}C NMR. The spectrum of dry GO (see Figure 1b) exhibits three characteristic resonance peaks at around 125, 67, and 55 ppm assigned to carbon−carbon double bonds

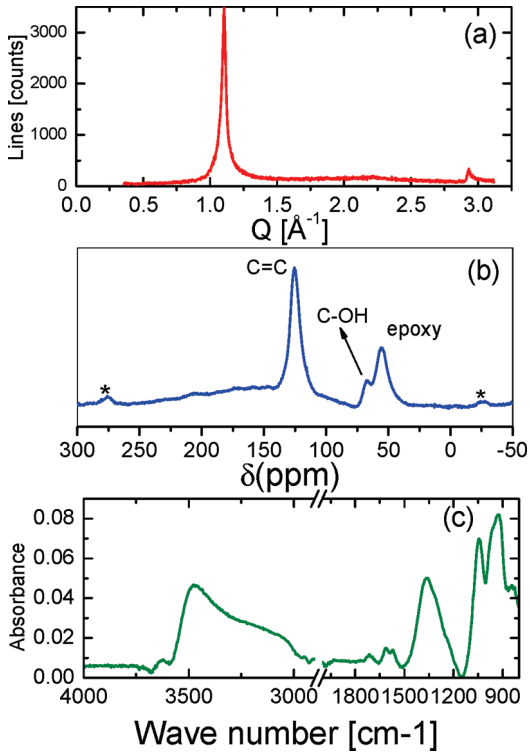

Figure 1. X-ray diffraction pattern (a), ^{13}C NMR spectrum (b), and ATR-FTIR spectrum in the range of 4000−3000 and 1800−900 cm^{-1} (c), of dry graphite oxide. In (b) the symbol * denotes the spinning side bands.

(C═C), hydroxyl groups (C−OH), and epoxy groups (C−O−C), respectively.[21–23,38–40] We have to mention that Mermoux et. al in ref 39 previously assigned the peak at about 60 ppm to the 1.3 ethers instead of epoxide groups.

Finally, FTIR-ATR spectroscopy gave additional information about the functional groups present in the surface of GO. Figure 1c shows the characteristic peaks of FTIR-ATR spectra of anhydrous GO where most of the bands overlap. A broad band ranging from 3650 to 3000 cm^{-1} indicates the presence of hydroxyl groups (3627 cm^{-1} stretching vibration of free hydroxyl groups of water, 3455 cm^{-1} stretching vibration of hydroxyl groups of GO). In addition, in the region of 3500−3560 cm^{-1} the OH stretching vibration of carboxyl groups is usually found. However, as the number of carboxyl groups is negligible, it will not be taken into consideration in the further analysis. In the intermediate region from 3000 to 2000 cm^{-1}, there is no visible bands although the spectra are very extended and some small feature is noted in the region of 2750 cm^{-1}. At around 1712 cm^{-1}, the stretching vibration of C═O from carboxylic groups, at 1055 cm^{-1} the stretching vibrations of C−O from ether and hydroxyl groups,[41] and at 1349 cm^{-1} the in-plane OH bending mode of hydroxyl groups[41] are observed. In 1570 cm^{-1}, the C═C aromatic ring stretching is visible. The origin of the band at 920 cm^{-1} is still discussed in the literature, but it is probably related with the epoxy groups in GO. Finally, a small feature at 1620 cm^{-1} is seen in the spectra, and it was assigned to the deformation vibration of the remaining adsorbed water molecules.[38,39,42]

Consequently, our GO contains a variable amount of hydroxyl, epoxy, carbonyl, and carboxylic groups similar to other GO synthesized and studied in the literature.[20,34,38] In spite of the fact that the exact structure of GO is still ambiguous, the carbonyl groups are probably mainly located at the edges of the carbon layers.[23,26]

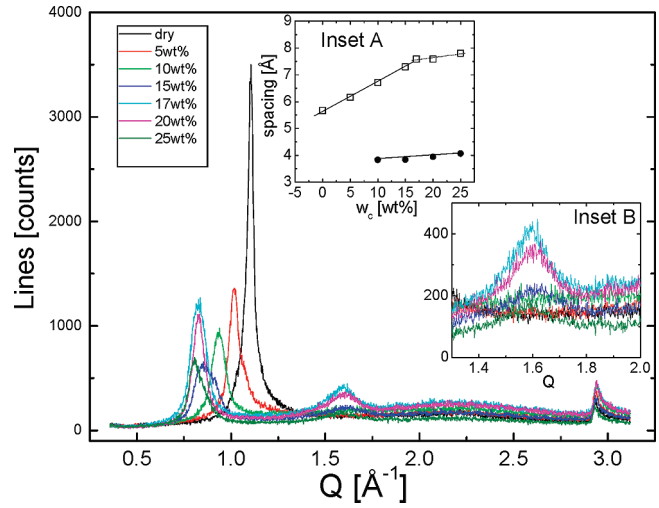

Figure 2. X-ray diffraction patterns of dry and hydrated GO as a function of the scattering vector (Q) at room temperature. Inset A: interlayer spacing (spacing) calculated from the main diffraction peak (open squares) and the second peak (full circles) as a function of water concentration. Inset B: X-ray diffraction data between 1.4 and 2 Å. This peak vanishes at low water concentration.

3.2. Structural Characterization of Hydrated GO. Figure 2 shows the powder X-ray diffraction patterns of GO at different hydration levels in comparison with the dry sample. Again, three typical peaks were observed for all the samples. Two of them (also observed in the dry GO) at about $Q = 2.93$ Å^{-1} ($2\theta = 43°$) and $Q = 2.22$ Å^{-1} ($2\theta = 31°$) are almost independent of water concentration. However, the observed peak at about $Q = 1.1$ Å^{-1} ($2\theta = 15°$) for the dry sample continuously shifts at lower Q-values as water content increases. In addition to these three diffraction peaks and for water concentrations higher than 10 wt %, a new diffraction peak is observed at around $Q = 1.6$ Å^{-1} ($2\theta = 23°$) (see inset B of Figure 2).

As mentioned above, the typical interlayer spacing for the main diffraction peak of dry GO was calculated, and the results are displayed in inset A of Figure 2 as a function of the water concentration. Clearly the spacing gradually increases up to a value of 8 Å. This growth in the spacing is an indication that water is intercalated between the galleries of the GO as observed also by other authors.[34,35] Also, the sharpness and intensity of this main diffraction peak decreased with increasing water concentration suggests a more heterogeneous structure.

ATR-FTIR was also performed on hydrated GO. Here we only focus in the region between 3800 and 3000 cm^{-1}, where the main absorption lines corresponding to the OH stretching vibration modes of water can be observed.[42] Figure 3 shows the comparison between the ATR-FTIR spectra for dry GO and the samples with a water content of 10 and 25 wt %, respectively. The broad band located between 3650 and 3000 cm^{-1} of dry GO is still present in the spectra, but its intensity clearly depends on water concentration. The inset of Figure 3 shows the difference between the spectrum of the hydrated GO and that of the dry GO. This allows extracting information about differences in the chemical environment between the samples with different water contents. Clearly, we found three bands located close to ∼3600, 3400, and ∼3200 cm^{-1} in both spectra. However, the intensity of the bands at 3600 and 3200 cm^{-1} significantly increases, whereas the band at approximately 3400 cm^{-1} shifts to lower frequencies (from 3470 cm^{-1} at 10 wt % to 3367 cm^{-1} at 25 wt %). Thus, the OH stretching region undergoes changes as a function of the hydration level.

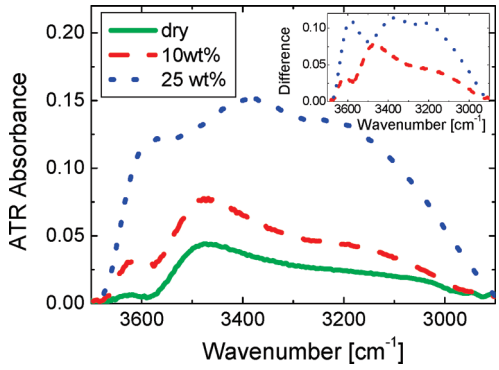

Figure 3. ATR-FTIR raw data of GO in the frequency range of 3700−2800 cm^{-1} where the OH stretching bands of water molecules are visible at room temperature. Inset: difference spectra between hydrated and anhydrous samples shown in this figure.

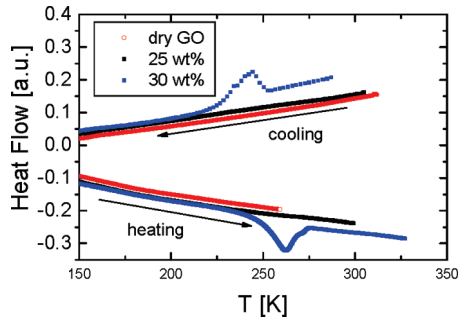

Figure 4. Heat flow measured by DSC during cooling and heating at a rate of 2 K/min for dry GO and water containing samples (c_w = 25 and 30 wt %). No calorimetric features are observed for both dry and c_w = 25 wt % samples. However, a crystallization and melting due to water crystallization are observed in the sample with c_w = 30 wt %. For this reason, we exclude in our study samples with a c_w > 25 wt %.

Finally, differential scanning calorimetry measurements were used to detect any feature in the thermal response of the samples (on cooling or heating). Figure 4 shows the heat flow of the anhydrous GO and samples with c_w = 25 and 30 wt % during cooling and heating at a rate of 2 K/min, respectively. From this figure, it is clear that there are no characteristic features in the calorimetric response (any crystallization/melting peak) for both the dry sample and that with c_w = 25 wt %. Note that this behavior is common for all the samples with c_w < 25 wt %. As a result, intercalated water in GO does not crystallize on cooling. At higher water concentration (30 wt %, see Figure 4), water crystallization on cooling and heating was revealed by DSC (about 4 wt % of ice). For this reason, samples with water concentration higher than 25 wt % were excluded of this study to make sure that intercalated water remains completely amorphous at supercooled temperatures.

3.3. Dynamical Behavior of Water Intercalated in GO. Figure 5a shows the imaginary part (ε'') of the complex permittivity at T = 150 K of hydrated GO having different water concentrations together with the response of the dry material. From Figure 5a it is clear that at low frequency conductivity effects dominates, whereas at higher frequencies a peak in the dielectric losses evidences a relaxation dynamics. In addition, we can observe that the amplitude of this peak increases with increasing water content. We have also to note (see Figure 5b) that, above 250 K, the intensity of the process slightly increases with temperature.

The relaxation process of the hydrated samples, shown in Figure 5 (a and b), was fitted with a symmetrical Cole−Cole (CC) function[43]

$$\varepsilon^*(\omega) = \varepsilon_\infty + \frac{\varepsilon_s - \varepsilon_\infty}{[1 + (i\omega\tau)^\alpha]} \quad (1)$$

where in eq 1 α is a shape parameter ($0 < \alpha \leq 1$); ε_∞ and ε_s are the unrelaxed and relaxed values of the dielectric permittivity; τ is a relaxation time; and ω is the angular frequency. Note that $\omega\tau = 1$ at the peak maximum. Additionally, it was necessary to add a power law term to account for the conductivity contribution at low frequencies. Moreover, at low temperatures (T < 180 K), an additional CC function was used to take into account the contribution of a new process on the right side of the main peak with a characteristic frequency outside of the frequency window. The relaxation strength of this faster component is very small compared with the relaxation strength of the main peak, and it is slightly dependent on water concentration. As this relaxation is not present in the dry sample, we can follow that it could be also related with the water molecules in the samples. Note that in other water-containing samples[45,46] this high-frequency component is also found. However, more studies are necessary to make a definitive assignment of this process. The inset in Figure 5a shows the dielectric response after conductivity subtraction. The relaxation strength corresponding to the main process in Figure 5 does not depend on temperature in this range, and a typical value is plotted as a function of water content in Figure 6 at 140 K. Additionally, α-values in eq 1 depend on temperature, and it varies approximately from 0.25 at 130 K to 0.48 at 240 K for all the samples.

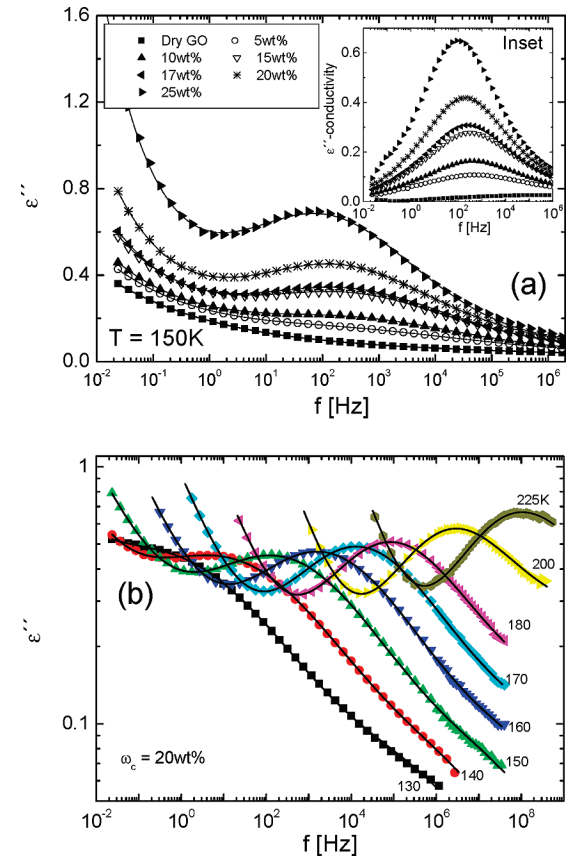

Figure 5. (a) Loss component, ε'', of the complex dielectric permittivity, $\varepsilon^*(f)$ of dried GO and at different water concentrations at 150 K. Inset: Data in this figure after subtraction of conductivity. (b) Loss component, ε'', of the complex dielectric permittivity, $\varepsilon^*(f)$, of GO with a water concentration of 20 wt %. The solid line through the data points is a least-squares fit to a superposition of a power law for conductivity and the imaginary part of two Cole−Cole functions (see text).

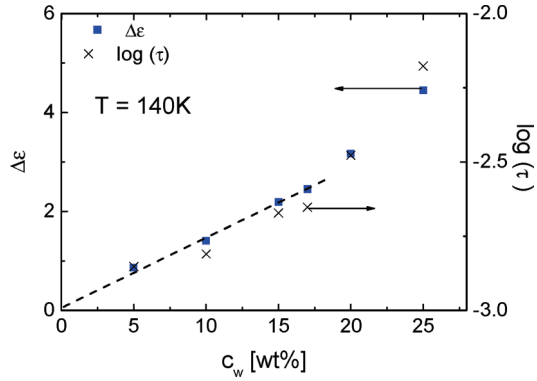

Figure 6. Dielectric strength ($\Delta\varepsilon$) and relaxation times (τ) versus water concentration for the main process observed in Figure 5 for all the water concentrations studied at $T = 140$ K.

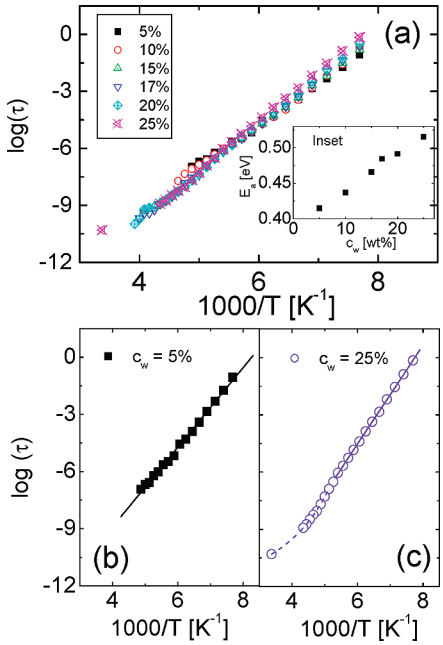

Figure 7. (a) Temperature dependence of the relaxation times for water confined in GO. Inset: activation energy (E_a) in a function of water content. (b) Temperature dependence of the relaxation times for $c_w = 5$ wt %. (c) Temperature dependence of the relaxation times for $c_w = 25$ wt %.

Figure 7(a) shows the temperature dependence of the relaxation times ($\tau = 1/(2\pi f_{max})$, where f_{max} is the frequency of the corresponding ε'' maximum) for all the water concentrations. As can be seen more clearly in Figure 7(b) and (c), the time scale of the main relaxation exhibits Arrhenius-type temperature dependence below approximately 180 K. However, at higher temperatures a slight deviation from the Arrhenius behavior was observed for the highest water contents. This behavior will be discussed in the next section. Thus, below 180 K, the relaxation times were fitted by the Arrhenius equation

$$\tau(T) = \tau_o \exp\left(\frac{E_a}{kT}\right) \quad (2)$$

where E_a represents a mean activation energy; k is the Boltzmann's constant; and τ_o is related to a molecular vibration time. Both E and $\log(\tau_o)$ are shown in Table 1, and it will also be discussed in the next section.

TABLE 1: Activation Energy (E_a) and Pre-Exponential Factor ($\log(\tau_o)$) Obtained from the Arrhenius Equation Applied to the Data In Figure 7[a]

c_w [wt %]	$\log(\tau_o[s])$	E_a [eV]
5	-17.3 ± 0.1	0.41
10	-17.9 ± 0.2	0.44
15	-17.9 ± 0.1	0.47
17	-19.4 ± 0.2	0.48
20	-19.6 ± 0.1	0.49
25	-20.1 ± 0.1	0.52

[a] The error in the activation energy was, on average, 0.1 eV.

Finally, to estimate the crossover temperature we have used the Arrhenius equation above presented to extrapolate the relaxation time at higher temperatures. This extrapolated relaxation time was fixed in a new fitting of the dielectric data. Above the crossover temperature, the resulting fitting is very poor. However, the best fitting results were with a faster relaxation time than that extrapolated with the Arrhenius equation. The crossover temperature (T_{cross}) was defined as the temperature where the extrapolated value of τ fails in obtaining a good fitting.

4. Discussion

As shown in Figure 2, the intercalation of water in GO is evident since the interlaying spacing grows from 5.7 Å (dry sample) up to 7.9 Å (sample with a water content of 25 wt %). In spite of the fact that the interlayer spacing depends on several factors such as the oxidation method, this result is consistent with other studies previously reported.[34,35]

The calorimetric and dielectric behavior of water molecules intercalated in GO can be summarized as follows. Water molecules intercalated in GO remain amorphous at low temperatures since DSC measurements show no signatures of crystallization. On the other hand, the relaxation strength of the water dielectric process moderately increases with water concentration up to $c_w = 15$ wt % (see Figure 6). However, at higher water concentrations ($c_w > 15$ wt %), a faster increase is observed in the relaxation strength. According to previous results of water solutions of several glass forming materials, sugars, and polymers,[44–46] this change in the concentration dependence of the relaxation strength can be interpreted as due to the existence of two different types of water: at low water concentration, water molecules would be strongly bound to the host molecules (graphene layer in the present case) being its reorientation highly restricted, whereas at higher water concentration, the rotational freedom of water increases probably because a significant amount of water is surrounded by other water molecules that are not in direct contact with the host molecules. So, the dynamics of water confined in GO changes across the two regimes at a water concentration around 17 wt %. It is worthy of remake that the characteristic relaxation times also show a similar behavior, as shown in Figure 6.

The above results found further confirmation when compared with the ATR-FTIR measurements in the 3600−3000 cm^{-1} range at 298 K (Figure 3). According to previous studies, the OH stretching band of bulk water can be decomposed into three main components[47–50] that could be attributing to three types of water species. Fully tetrahedrally coordinated hydrogen-bonded water molecules contribute to the intensity at about 3200 cm^{-1} and represent the bulk-like structure of water or the so-called "network water".[51] Weakly hydrogen-bonded water appears at higher frequencies (near 3600 cm^{-1}), and it corresponds to small

water aggregates or water having no contacts with other water molecules.[48,49,52] Between these two extremes, there are water molecules in an environment of partial hydrogen bonds that contribute to the infrared spectra at intermediate frequencies (at about 3400 cm^{-1}), and it could reflect the interaction of water molecules with a solute, surface, or a confining environment.[47,49] In our case, a high increment is observed in the band near 3200 cm^{-1} indicating the presence of water molecules highly coordinated at high water concentration. This behavior is in accordance with the dielectric response which seems to be dominated by water−water interactions. In addition, the maximum of the band at 3468 cm^{-1} in the low hydration regime shifts to lower wavenumber (~3390 cm^{-1}) also indicating that water molecules intercalated in GO are gradually involved in arrangements with an increasing number of hydrogen bonding partners. Finally, the intensity of the band at 3600 cm^{-1} in the sample with the higher water content also increases. This is congruent with an increment in the fraction of weakly hydrogen-bonded species as compared with the sample with low water content, and it could indicate that there are species that remain almost isolated, maybe in the space between the functional groups or attached to groups at the edges of GO. This result is in agreement with molecular dynamics simulations of water adsorption on activated carbons.[53] In that case, it was shown that water adsorbs preferentially on active sites on the surface, and these adsorbed molecules act as nucleation sites for further adsorption of water, forming three-dimensional clusters.[53]

More structural related information can be extracted from the X-ray measurements shown in Figure 2. As mentioned above, a diffraction peak (at $Q = 1.6$ $Å^{-1}$) emerges in the spectra at water concentration higher than 10 wt %. This fact could also be related with the appearance of water domains. To improve the analysis of this new diffraction characteristic, we prepared a sample with $c_w = 25$ wt % and recorded the diffraction spectra from $Q = 0.25$ to 2 $Å^{-1}$ during the course of dehydration (note that our dielectric samples were prepared in this way). The results are shown in Figure 8 (a and b) where all the features can be analyzed during the dehydration time. At $t = 0$ (when the sample contains 25 wt % of water), three characteristic peaks can be seen in the X-ray spectra. The Q-peak at 2.93 $Å^{-1}$ does not shift with water content (not shown in the Figure 8). However, during the dehydration, the intermediate peak "disappears" (in the sense that the area of the Lorentian function used to fit the spectra goes to zero) leaving only two characteristic peaks similar to the dried GO. This fact can be simply explained as follows: during the hydration process, the intercalated water causes a progressive increase of the interlayer spacing from 6 to 7 Å. We have to note that partially or completely empty interlayer spaces could be present as noted by other authors.[34,53] At hydration levels higher than 10 wt %, it seems that water molecules could have a preference to bond with other water molecules, instead to hydrate a partially filled or an empty layer, in agreement with the hydration mechanism discussed above.[53] During this process, the empty spaces in GO would collapse, giving an intermediate spacing value of 4 Å. Thus, as shown above for both the behavior of the dielectric strength and the infrared spectra, X-ray measurements indicate a structural alteration with increasing water concentration that could be associated with the appearance of water domains.

Now, we focus on the activation energy obtained from the Arrhenius behavior plotted in the inset of Figure 7a. The activation energy slightly increases with the hydration level, from 0.42 eV at 5 wt % to 0.51 eV at 25 wt %. These values are in agreement with the previously published results in aqueous

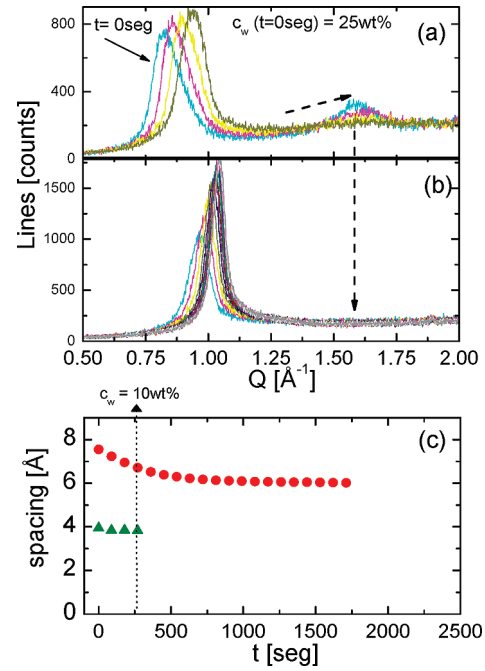

Figure 8. (a) and (b) Time-resolved X-ray diffraction of 25 wt % GO dehydration. The curves from left to right were registered every 35 s representing the dehydration of GO in the time. (a) The first four curves recorded in the time show the displacement of the main diffraction peak to higher Q and the intensity reduction of the secondary peak. (b) Subsequent diffractograms recorded after those plotted in graph "a" showing the increase of the intensity of the main diffraction peak and the disappearance of the secondary peak. (c) Interlayer spacing of GO as a function of dehydration time calculated from the main and secondary diffraction peaks.

solutions of polymers and glass forming systems.[44,54] Moreover, a universal behavior at high water concentration for the temperature dependence of the relaxation times in these solutions was proposed, which is found to be also valid for water intercalated in GO. The increase of the activation energy with the hydration level can be attributed to an increasing number of hydrogen bonding partners. This interpretation is also in good agreement with the above results obtained by all the different techniques.

4.1. Relaxation Times: Comparison with NS Results. First of all, we compare the temperature dependence of the relaxation times in the high hydration regime and at high temperatures with that obtained by Buchsteiner et. al by using neutron scattering (NS) techniques[34,35] on the same system. Note that the GO used in this work could have a different atomic composition from that used in refs 34 and 35 since the preparation methods are different. This fact could have an impact on the water dynamics analyzed in these two systems.

The sample hydrated in an atmosphere with a relative humidity of 75% has an interlayer distance close to 8 Å in ref 34, similar to the sample with a water concentration of 25 wt % in this work which suggests similar water content. For this reason, we chose to compare these two samples. Figure 9(a) shows the comparison of the relaxation times obtained by using these two different techniques. In spite of the fact that both techniques probe different physical properties and probably both samples have not exactly the same water content and the GO itself could be different, the agreement is quite good. Thus, we can conclude that both techniques qualitatively evidence the same results in the temperature interval analyzed. Note also that from quasielastic neutron scattering techniques it was possible to detect a faster relaxation (open squares in Figure 9(a)) which

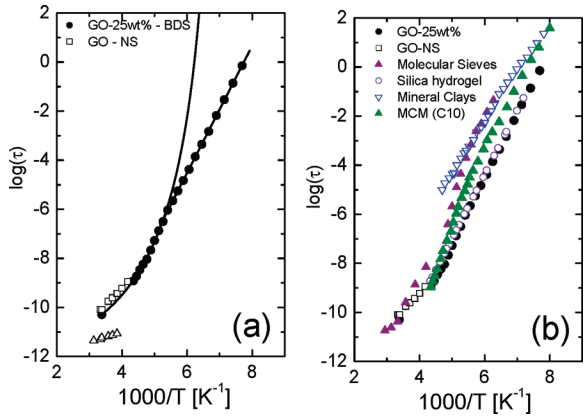

Figure 9. (a) Temperature dependence of the relaxation times for 25 wt % water content (solids symbols) and those obtained from neutron scattering (open symbols) in ref 34. (b) Temperature dependence of the relaxation times for confined water in different systems: vermiculite clay,[11] MCM-41,[58] silica gel,[55] and molecular sieves.[56]

is outside of the dielectric frequency window. Buchsteiner et. al[34] interpreted their results for the sample with an interlayer distance of 8 Å, in terms of a model that combines double two-site jump motions due to the motions of the whole molecule and the motions of OH groups, respectively. The faster processes shown in Figure 9a (jump 2 or short jumps in ref 34) were attributed to 180° flips of isolated water molecules in the interlayer space of GO, whereas the slower process (jump 1 or long jumps in ref 34) was assigned to long jump motion of the hydrogen atom of the OH groups between two positions of oxygen atoms in GO (either epoxide or OH-groups), which should both belong to the next graphite oxide layer for most of the jumps. Conversely dielectric spectroscopy, that probes reorientation motions of polar molecules, shows that the slower process also seen by NS is directly related with water molecule reorientation (see Figure 5). It is therefore unlikely that this process only involves OH groups from GO. Moreover, as mentioned above the temperature dependence of the BDS relaxation times shows a non-Arrhenius behavior (see full line in Figure 9a) indicating an onset of cooperative motions of water molecules, evidenced at a hydration level higher than 17 wt % when there could be enough water molecules to form the H-bonded network necessary for cooperative motions.

Finally, we have to mention that at water concentration higher than approximately 15 wt % the relaxation times show a crossover between non-Arrhenius to Arrhenius behavior in the temperature range between 190 and 200 K.

4.2. Temperature Dependence of the Relaxation Times: Comparison with Other Confinement Systems. Confined water generally shows structural, thermodynamic, and dynamical properties different from bulk water due to interactions with confining surfaces. In particular, the confined water dynamics was intensely studied by various experimental techniques using different host materials as well as by computer simulations.[11–19] These studies have shown that the temperature dependence of the relaxation time of confined water in all these systems depicted a crossover from a non-Arrhenius to an Arrhenius behavior at certain temperature, T_{cross}. In some cases, this crossover was found to be dramatic;[16,18,19] however, in other cases the crossover is only slightly noted (such as in the present case of GO), and there are also cases where the crossover is not detected at all.[11,55,56]

Table 2 summarizes some of the values published in the last years on water dynamics in well-defined confinement systems as measured by dielectric spectroscopy. In addition, Figure 9(b) shows the temperature dependence of the relaxation times taken from these references. Certainly, the type of confinement and the nature of the pore system may have an impact on the observations made and their interpretations. In some cases, water molecules strongly interact with the confining host material through hydrogen bonding, and, in other cases the confining material presents hydrophobic actives sites (see Table 2). However, we can find some common behavior by analyzing the temperature dependence of the relaxation times in Figures 9(b). The crossover is observed at temperatures between 180 and 205 K in all these diverse confinement systems. The observed crossover is detected on the relaxation map as a moderate change in the temperature dependence behavior. Thus, we can conclude that the crossover observed by BDS is gradual, and it does not show a discontinuous behavior between these two regimes. Consequently, these results are not concerned with the possible existence of a sudden change as that observed by NS techniques at $T_{cross} = 220$ K in similar confinement systems.[13,18,19] In fact, BDS data do not show any crossover in the temperature region of 200−240 K. Thus, we cannot directly relate the presence of the crossover in the BDS data with the possible existence of an FTS transition proposed for bulk water. However, we found a possible explanation for the dielectric detected crossover comparing these systems with normal glass forming liquids.

In several theories of the glass transition,[59] it is assumed that the dynamics of glass-forming liquids is governed by the collective motions of molecules over a length scale, ξ (the cooperative length), which increases with decreasing temperature. The dramatic slowing down of molecular motions in glass-forming materials is attributed to this increase of ξ. In this view, the glass transition (T_g) occurs when the cooperative length cannot further increase, and therefore the cooperative molecular movements become frozen. The same idea could be applied to the interpretation of the dielectric data of water intercalated in GO shown in Figure 7. At high temperatures, the small clusters of water molecules cooperatively move, and the relaxation times follow a non-Arrhenius behavior. On cooling, the system reaches T_{cross} where the cooperative motions become restricted since the cooperative length can no longer increase because of the presence of the confining host material. Below T_{cross}, the time response will follow the Arrhenius behavior. In this context, the observed crossover is the expression of a change from liquid-like dynamics toward a confined-like behavior at T_{cross}. In agreement with this analysis, it has been established that the water relaxation observed in different kinds of soft confinements at high hydration level (when water−water interactions become relevant)[44,45] has the characteristics of a secondary or β-like relaxation with an average activation energy of (0.54 ± 0.04) eV. Note that also collagen and elastin studied by BDS show the same activation energy at several hydrations.[60] We found almost the same activation energy (see Table 1) for water intercalated in GO (see Figure 9(b)), and in addition, the relaxation is broad and symmetric. Consequently, due to the similarities found in these systems, we can follow that the water relaxation observed in Figure 7 at temperatures lower than T_{cross} has the characteristics of a secondary relaxation. This result is also in agreement with studies by ^{2}H NMR in both elastin and collagen,[61] solutions of several systems at low hydration level,[62] and for hydrated proteins.[63] Interestingly, and in agreement with these results, other workers[64] argued that the process showing a crossover to Arrhenius behavior at low temperatures has the characteristic of a Johari−Goldstein relaxation (JG).[65,66] Often, the frequency-dependent dielectric data of supercooled liquids

TABLE 2: Compilation of Parameters Related with Experiments of Water Confined in Well-Defined Confinement Systems[a]

system	Dm	D [Å]	ET	c_w	T_{cross} [K]	E_a [eV]	ref
mineral clays	2	14.96	DS	two water layer	not reported	0.48	11
hydrogel (silica matrix)	3	–	DS	$0.7grH_2O/grSiO_2$	not reported	0.51	55
molecular sieves	2	10	DS, NS	full hydration	185	0.50	57
MCM41-C10	2	21	DS	full hydration levels	180	0.48	58
		36					
graphite oxide	2	8	DS	one water layer	192	0.52	this work

[a] Relaxations times are displayed in Figure 9b. Dm, dimensionality; D, diameter; ET, Experimental technique; c_w, water concentration; T_{cross}, crossover temperature; DS, dielectric spectroscopy; and NS, neutron scattering.

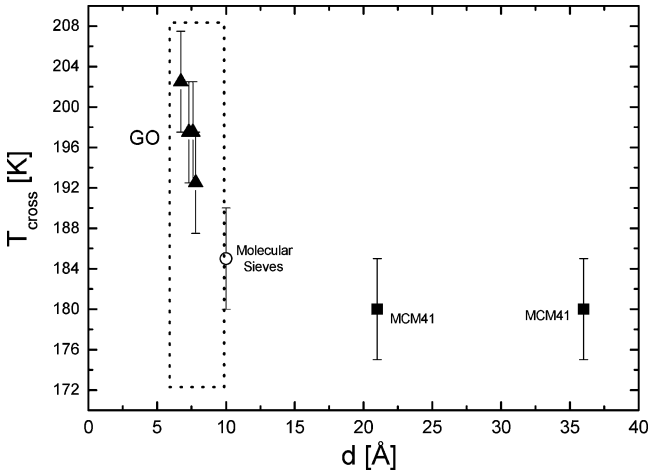

Figure 10. Crossover temperature (T_{cross}) versus the confinement length for different confinement systems: GO (triangles, this work), MCM-41 (squares[58]), and molecular sieves (circles[56]). T_{cross} is independent of the confinement length for $d > 10$ Å.

display relaxations beyond the structural relaxation associated with the glass transition (α-relaxation). The molecular mechanism of these secondary relaxations can be intermolecular (for example, the local motion of the whole molecule) or intramolecular (for instance, the rotation of a lateral group in a polymeric chain). The intermolecular relaxations are generally referred to as Johari−Goldstein relaxation which would correspond to relaxations taking place in loosely packed regions in the glassy state, i.e., the so-called "island of mobility" in the seminal work of Johari−Goldstein. Note that the picture presented above for water dynamics confined in GO at low temperature can also be viewed as "island of mobility". In summary, the here proposed interpretation of our dielectric data and that given in ref 64 are somehow compatible. However, no association with the interpretation of island of mobility was made by the authors of ref 64.

More evidence can be found by analyzing the behavior of the crossover temperature as a function of the confinement length (d) for different geometrical confinements. Figure 10 shows the variation of T_{cross} with d. T_{cross} varies for confinement lengths smaller than 10 Å. However, no shift, within the experimental error, in the crossover temperature is observed for confinement lengths larger than 10 Å. As a consequence, it seems that size effects influence the crossover temperature only for a confinement distance lower than approximately 10 Å. This result is in agreement with molecular dynamics simulations of water in hydrophilic silica surfaces where confinement-independent profiles for the dynamic properties are observed at $d > 6$ Å[67] and with most of the observations in ultrathin polymers films[68,69] and polymer blends[70,71] in which the dynamic properties, as measured by BDS, do not change for confinement lengths higher than 10 Å. Therefore, supercooled water in different kinds of hydrophilic confinements behaves as other supercooled liquids. Note that this could be the case of water solutions in the high hydration level, where the crossover is produced at the glass transition temperature as measured by DSC ($T_{cross} = T_{g,sol}$).[44–46] In that case, the features observed in the relaxation map are a consequence of the existence of constraints imposed by the glassy matrix.

On the other hand, the situation for confinement sizes higher than 10 Å seems to be different since finite size effects are not noticeable, and therefore the observed water dynamics could be related with intrinsic water properties of confined water in hydrophilic environments, although it could also be influenced by the specific surface interaction.[72]

Finally, note that for confinement lengths smaller than 10 Å, confinement size effects emerge in the dynamical response, whereas for confinement lengths bigger than 20 Å it is not possible to avoid crystallization of water on cooling. Therefore, it seems that for the study of intrinsic properties of confined water in hydrophilic environments, an appropriate confinement size should be restricted to a window between 10 and 20 Å.

5. Conclusion

We have studied the water dynamics intercalated in GO. While the dry sample showed no relaxation process, the water-containing samples showed a relaxation process attributed to water molecules. As in other water-containing samples, the relaxation strength increases more rapidly for water concentration higher than 15 wt %. This is an indirect indication that water domains of significant size are present in the samples. In agreement with this result, ATR-FTIR spectra in the range of 3600−3000 cm^{-1} showed a marked shift in the position of the peaks indicating that water is progressively highly coordinated with increasing water concentration, supporting the presence of water clusters in the samples at high hydration level.

As in other confinement systems studied by BDS, the temperature dependence of the relaxation times shows a crossover from non-Arrhenius to Arrhenius at T_{cross}. By analyzing different confinement systems we conclude that for water molecules restricted at lengths scales lower than 10 Å finite size effects are detected, whereas at higher confinement lengths, finite size effects are not disturbing the dynamical observation. However, this length cannot increase too much since water crystallization would appear in the samples. Therefore, we suggest that an appropriated confinement length to study the dynamical water properties, in this utmost important temperature range (240 K < T < 150 K), is from 10 to approximately 20 Å. In this way, no finite size effects would take place, and crystallization could be avoided.

Acknowledgment. The authors gratefully acknowledge the support of the Spanish Ministry of Education, project CSD2006-00053; the European Union, project 502235-2; and SOFTCOMP program and the Basque Government, and project IT-436-07.

Supporting Information Available: The thermal decomposition of GO prepared in this work through Brodie's method was analyzed by TGA at 110 °C during 6 days. As can be seen, no appreciable degradation appears in the GO prepared with this method. This material is available free of charge via the Internet at http://pubs.acs.org.

References and Notes

(1) Hecht, A. M.; Geissler, E. *J. Colloid Interface Sci.* **1970**, *34*, 32.
(2) Woessner, D. E.; Snowden, B. S.; Chiu, Y. C. *J. Colloid Interface Sci.* **1970**, *34*, 283.
(3) Woessner, D. E.; Snowden, B. S. *J. Colloid Interface Sci.* **1970**, *34*, 290.
(4) Hougardy, J.; Stone, W. E. E.; Fripiat, J. J. *J. Chem. Phys.* **1976**, *64*, 3840.
(5) Alcoutlabi, M.; McKenna, G. B. *J. Phys.: Condens. Matter* **2005**, *17*, R461.
(6) Jackson, C. L.; McKenna, G. B. *J. Non-Cryst. Solids* **1991**, *131*−*133*, 221.
(7) Bellissent-Funel, M. C. *Eur. Phys. J. E* **2003**, *83*, 92.
(8) Alba-Simionesco, C.; Coasne, B.; Dosseh, G.; Dudziak, G.; Gubbins, K. E.; Radhakrishnan, R.; Sliwinska-Bartkowiak, M. *J. Phys.: Condens. Matter* **2006**, *18*, R15.
(9) Gelb, L. D.; Gubbins, K. E.; Radhakrishnan, R.; Sliwinska-Bartkowiak, M. *Rep. Prog. Phys.* **1999**, *62*, 1573.
(10) Bhattacharyya, K.; Bagchi, B. *J. Phys. Chem. A* **2000**, *104*, 10603.
(11) Swenson, J.; Bergman, R. *Nature* **2000**, *403*, 6767.
(12) Zanotti, J. M.; Bellissent-Funel, M. C.; Chen, S. H. *Phys. Rev. E* **1999**, *59*, 3084–3093.
(13) Chen, S. H.; Liu, L.; Faraone, A. *Phys. Rev. Lett.* **2006**, *97*, 189803.
(14) Angell, C. A. *J. Non-Cryst. Solids* **1991**, *131*−*133*, 13–31.
(15) Ito, K.; Moynihan, C. T.; Angell, C. A. *Nature (London)* **1999**, *398*, 492.
(16) Faraone, A.; Liu, L.; Mou, C. Y.; Yen, C. W.; Chen, S. H. *J. Chem. Phys.* **2004**, *121*, 10843.
(17) Oguni, M.; Kanke, Y.; Namba, S. *AIP Conf. Proc.* **2008**, *982*, 34–38.
(18) Zhang, Y.; Lagi, M.; Ridi, F.; Fratini, E.; Baglioni, P.; Mamontov, E.; Chen, S. H. *J. Phys.: Condens. Matter* **2008**, *20*, 502101.
(19) Mamontov, E.; Burnham, C. J.; Chen, S. H.; Moravsky, A. P.; Loong, C. K. *J. Chem. Phys.* **2006**, *124*, 194703.
(20) Brodie, B. C. *Ann. Chim. Phys.* **1860**, *59*, 466.
(21) Mermoux, M.; Chabre, Y.; Rousseau, A. *Carbon* **1991**, *29*, 469–474.
(22) He, H. Y.; Riedl, T.; Lerf, A.; Klinowski, J. *J. Phys. Chem.* **1996**, *100*, 19954–19958.
(23) Lerf, A.; He, H. Y.; Forster, M.; Klinowski, J. *J. Phys. Chem. B* **1998**, *102*, 4477–4482.
(24) Lahaye, R. J. W. E.; Jeong, H. K.; Park, C. Y.; Lee, Y. H. *Phys. Rev. B* **2009**, *79*, 125435.
(25) Khare, R.; Mielke, S. L.; Paci, J. T.; Zhang, S. L.; Ballarini, R.; Schatz, G. C.; Belytschko, T. *Phys. Rev. B* **2007**, *75*, 075412.
(26) Boukhvalov, D. W.; Katsnelson, M. I. *J. Am. Chem. Soc.* **2008**, *130*, 10697–10701.
(27) Nakajima, T.; Mabuchi, A.; Hagiwara, R. *Carbon* **1988**, *26*, 357.
(28) Li, Z.; Zhang, W.; Luo, Y.; Yang, J.; Guo Hou, J. *J. Am. Chem. Soc.* **2009**, *131*, 6320–6321.
(29) Matsuo, Y.; Tahara, Y. K.; Sugie, Y. *Carbon* **1997**, *35*, 113–120.
(30) Matsuo, Y.; Hatase, K.; Sugie, Y. *Chem. Mater.* **1998**, *10*, 2266–2269.
(31) Liu, P. G.; Gong, K. C.; Xiao, P.; Xiao, M. *J. Mater. Chem.* **2000**, *10*, 933–935.
(32) Bissessur, R.; Scully, S. F. *Solid State Ionics* **2007**, *178*, 877–882.
(33) Zong-huai, L.; Zheng-Ming, W.; Xiaojing, Y.; Kenta, O. *Langmuir* **2002**, *18*, 4926–4932.
(34) Buchsteiner, A.; Lerf, A.; Pieper, J. *J. Phys. Chem. B* **2006**, *110*, 22328.
(35) Lerf, A.; Buchsteiner, A.; Pieper, J.; Schottl, S.; Dekany, I.; Szabo, T.; Boehm, H. P. *J. Phys. Chem. Solids* **2006**, *67*, 106–1110.
(36) Barroso-Bujans, F.; Cerveny, S.; Verdejo, R.; del Val, J. J.; Alberdi, J. M.; Alegría, A.; Colmenero, J. *Carbon* **2009**, *48*, 1079−1087.
(37) Hamwi, A.; Marchand, V. *J. Phys. Chem. Solids* **1996**, *57*, 867–872.
(38) Hontoria-Lucas, C.; Lopez-Peinado, A. J.; De, J.; Rojas-Cervantes, M. L.; Martín-Aranda, R. M. *Carbon* **1995**, *33*, 1585–1592.
(39) Mermoux, M.; Chabre, Y. *Synth. Met.* **1989**, *34*, 157.
(40) Titelman, G. I.; Gelman, V.; Bron, S.; Khalfin, R. L.; Cohen, Y.; Bianco-Peled, H. *Carbon* **2005**, *43*, 641–649.
(41) Bellamy, L. J. *The Infrared Spectra of Complex Molecules*; Chapman and Hall: London, 1975.
(42) Jeong, H. K.; Noh, H. L.; Kim, J. Y.; Jin, M. H.; Park, C. Y.; Lee, Y. H. *Europhys. Lett.* **2008**, *82*, 67004.
(43) Cole, R. H.; Cole, K. S. *J. Chem. Phys.* **1942**, *10*, 98.
(44) Cerveny, S.; Alegría, A.; Colmenero, J. *Phys. Rev. E* **2008**, *77*, 031803.
(45) Cerveny, S.; Alegría, A.; Colmenero, J. *J. Chem. Phys.* **2008**, *128*, 044901.
(46) Cerveny, S.; Colmenero, J.; Alegría, A. *Macromolecules* **2005**, *38*, 7056.
(47) Crupi, V.; Longo, F.; Majolino, D.; Venuti, V. *J. Chem. Phys.* **2005**, *123*, 154702.
(48) Boissire, C.; Brubach, J. B.; Mermet, A.; de Marzi, G.; Bourgaux, C.; Prouzet, E.; Roy, P. *J. Phys. Chem. B* **2002**, *106*, 1032.
(49) Crupi, V.; Longo, F.; Majolino, D.; Venuti, V. *J. Phys.: Condens. Matter* **2006**, *18*, 3563.
(50) Jain, T. K.; Varshney, M.; Maitra, A. *J. Phys. Chem.* **1989**, *93*, 7409.
(51) Stanley, H. E.; Texeira, J. *J. Chem. Phys.* **1980**, *73*, 3404.
(52) Rousset, J. L.; Duval, E.; Boukenter, A. *J. Chem. Phys.* **1990**, *92*, 2150.
(53) Müller, E. A.; Rull, L. F.; Vega, L. F.; Gubbins, K. E. *J. Phys. Chem.* **1996**, *100*, 1189.
(54) Cerveny, S.; Alegria, A.; Colmenero, J. *Eur. Phys. J.-Spec. Top.* **2007**, *141*, 49.
(55) Cammarata, M.; Levantino, M.; Cupane, A.; Longo, A.; Martorana, A.; Bruni, F. *Eur. Phys. J. E* **2003**, *12*, 16.
(56) Schiró, G.; Cupane, A.; Pagnotta, S. E.; Bruni, F. *J. Non-Cryst. Solids* **2007**, *353*, 4546.
(57) Jansson, H.; Swenson, J. *Eur. Phys. J. E* **2003**, *12*, 13.
(58) Sjostrom, J.; Swenson, J.; Bergman, R.; Kittaka, S. *J. Chem. Phys.* **2008**, *128*, 154503.
(59) Donth, E. *The glass transition relaxation dynamics in liquids and disordered materials*; Springer: Berlin, 2001.
(60) Gainaru, C.; Fillmer, A.; Böhmer, R. *J. Phys. Chem. B* **2009**, *113*, 12628.
(61) Vogel, M. *Phys. Rev. Lett.* **2008**, *101*, 225701. *J. Phys. Chem. B* **2009**, *113*, 9386.
(62) Cerveny, S.; Schwartz, G. A.; Bergman, R.; Swenson, J. *Phys. Rev. Lett.* **2004**, *93*, 245702.
(63) Swenson, J.; Jansson, H.; Bergman, R. *Phys. Rev. Lett.* **2006**, *96*, 247802.
(64) Capaccioli, S.; Ngai, K. L.; Shinyashiki, N. *J. Phys. Chem. B* **2007**, *111*, 8197. Ngai, K. L.; Capaccioli, S.; Shinyashiki, N. *J. Phys. Chem. B* **2008**, *112*, 3826.
(65) Johari, G. P.; Goldstein, M. *J. Chem. Phys.* **1970**, *53*, 2372.
(66) Power, G.; Vij, J. K.; Johari, G. P. *J. Chem. Phys.* **2006**, *124*, 074509.
(67) Romero-Vargas, S.; Giovambattista, N.; Aksay, I. A. *J. Phys. Chem B* **2009**, *113*, 7973.
(68) Labahn, D.; Mix, R.; Schönhals, A. *Phys. Rev. E* **2009**, *79*, 011801.
(69) Serghei, A.; Huth, H.; Schick, C.; Kremer, F. *Macromolecules* **2008**, *41*, 3636.
(70) Cangialosi, D.; Alegria, A.; Colmenero, J. *Phys. Rev. E* **2007**, *76*, 011514.
(71) Schwartz, G. A.; Cangialosi, D.; Alegria, A.; Colmenero, C. *J. Chem. Phys.* **2006**, *124*, 154904.
(72) He, F.; Wang, L.-M.; Richert, R. *Eur. Phys. J.-Spec. Top.* **2007**, *141*, 3.

JP907979V